Published in final edited form as:
Biomaterials. 2012 July ; 33(21): 5247–5258. doi:10.1016/j.biomaterials.2012.03.076.

A functional agarose-hydroxyapatite scaffold for osteochondral interface regeneration

Nora T. Khanarian, **Nora M. Haney**, **Rachel A. Burga**, and **Helen H. Lu***
Biomaterials and Interface Tissue Engineering Laboratory, Department of Biomedical Engineering, Columbia University, 1210 Amsterdam Avenue, 351 Engineering Terrace, MC 8904, NY 10027, USA

Abstract

Regeneration of the osteochondral interface is critical for integrative and functional cartilage repair. This study focuses on the design and optimization of a hydrogel-ceramic composite scaffold of agarose and hydroxyapatite (HA) for calcified cartilage formation. The first study objective was to compare the effects of HA on non-hypertrophic and hypertrophic chondrocytes cultured in the composite scaffold. Specifically, cell growth, biosynthesis, hypertrophy, and scaffold mechanical properties were evaluated. Next, the ceramic phase of the scaffold was optimized in terms of particle size (200 nm vs. 25 μm) and dose (0–6 w/v%). It was observed that while deep zone chondrocyte (DZC) biosynthesis and hypertrophy remained unaffected, hypertrophic chondrocytes measured higher matrix deposition and mineralization potential with the addition of HA. Most importantly, higher matrix content translated into significant increases in both compressive and shear mechanical properties. While cell hypertrophy was independent of ceramic size, matrix deposition was higher only with the addition of micron-sized ceramic particles. In addition, the highest matrix content, mechanical properties and mineralization potential were found in scaffolds with 3% micro-HA, which approximates both the mineral aggregate size and content of the native interface. These results demonstrate that the biomimetic hydrogel-ceramic composite is optimal for calcified cartilage formation and is a promising design strategy for osteochondral interface regeneration.

Keywords

Biomimetic material; Chondrocyte; Hydrogel; Hydroxyapatite composite

1. Introduction

Osteoarthritis is a degenerative joint disease that is characterized by lesions of articular cartilage, which often lead to severe pain and loss of joint function. Since cartilage has a limited capacity for self-repair [1], surgical intervention is required to treat this debilitating condition. Current procedures include joint lavage, periosteal grafts, subchondral drilling, or microfracture. However, poor long-term outcomes are associated with many of these techniques due to unwanted fibrocartilage formation and inadequate graft-to-bone integration [2–4]. A variety of hydrogel-based, tissue engineered cartilage grafts have been investigated for cartilage repair [5–12]. While initial results are promising, consistent and systematic regeneration of the interface between the graft and subchondral bone remains a challenge. The native osteochondral interface is comprised of a calcified cartilage layer,

*Corresponding author. Tel.: +1 212 854 4071 (office); fax: +1 212 854 8725. hl2052@columbia.edu (H.H. Lu).

within which hypertrophic chondrocytes are embedded in a mineralized matrix of types II and X collagen, as well as proteoglycans [13–15]. In addition to facilitating cartilage-to-bone integration, the osteochondral interface also serves as a physical barrier that enables pressurization of articular cartilage, while curtailing vascular invasion from bone [16–18]. Such a barrier is essential for maintaining the integrity of repaired cartilage over time and has been shown to prevent osseous upgrowth in full-thickness defects [19]. Therefore, regeneration of the calcified cartilage layer is a prerequisite for functional and integrative cartilage repair.

The ideal osteochondral interface scaffold must promote the formation of a calcified cartilage matrix with physiologically relevant mechanical properties. This study focuses on the design and optimization of a hydrogel-ceramic composite scaffold for osteochondral interface tissue engineering. By pre-incorporating a hydroxyapatite (HA) phase into a hydrogel, scaffold mechanical properties and osteointegration can be enhanced. For example, HA particles embedded in alginate were shown to support chondrocyte viability, collagen deposition, and hypertrophy [20]. While these results are promising and demonstrate the feasibility of hydrogelceramic composites for osteochondral interface regeneration, the alginate-HA system has several limitations. First, the relatively long gelation time of alginate, which is controlled by the inward diffusion of divalent cations, allows HA particles to aggregate at the bottom of the gel. It is therefore difficult to control HA distribution in alginate. Secondly, given the ionotropic nature of alginate, whereby cross-linking is achieved most commonly with calcium ions, it would be more optimal to have a scaffold system whose calcium content is modulated only with the pre-incorporation of HA particles. Another limitation of the alginate-HA scaffold is that its mechanical properties are substantially lower than that of cartilage or the native osteochondral interface. To address these concerns, the objective of this study is to design and optimize an agarose-HA composite scaffold for osteochondral interface tissue engineering. Similar to alginate, agarose is a well-characterized hydrogel that has been used extensively for chondrocyte culture and cartilage tissue engineering [21–24]. Moreover, physiologically relevant mechanical properties which approach those of the native cartilage have been reported with chondrocyte-laden agarose constructs [21,25].

In this study, the hydrogel-composite scaffold will be optimized based on cell type, HA size, and dose for formation of a calcified cartilage-like matrix *in vitro*. The first objective of this study is to compare the response of interface-relevant cells in HA-free and HA containing agarose scaffolds. While deep zone chondrocytes (DZC) have been utilized for regeneration of calcified cartilage [20,26–28], hypertrophic chondrocytes are the resident cell population identified at the native osteochondral interface [29]. In this study, to induce DZC hypertrophy, thyroid hormone (T3) will be used to stimulate cell alkaline phosphatase activity and upregulate collagen X expression [30,31]. It is hypothesized that compared to DZC, the induced hypertrophic chondrocytes (DZC + T3) will better support the formation of a calcified cartilage-like matrix in HA-containing agarose scaffolds.

The second objective of the study is to optimize the hydrogelceramic composite scaffold in terms of HA particle size and dose. At the native osteochondral interface, chondrocytes are embedded within a calcified matrix, which is comprised of HA crystals on the order of 15–20 nm, as well as micron-sized HA aggregates [32,33]. Therefore, the effects of incorporating nano- versus micron-sized HA particles in agarose scaffolds will be investigated, with size-dependent responses anticipated for hypertrophic chondrocytes. In addition to particle size, the dose-dependent effects of HA particles will be investigated in this study. The calcium content of native calcified cartilage has been estimated to range from 1 to 28% of dry weight [34]. Therefore a dose-dependent effect on cell response is anticipated, and given that mineral content correlates positively with tissue mechanical

properties [35], it is expected that scaffold mechanical properties will also be modulated by HA dose. Findings from these studies will enable the identification of optimal parameters (cell type, HA size, dose) for biomimetic interface scaffold design and the formation of calcified cartilage *in vitro*.

2. Materials and methods

2.1. Cells and cell culture

Primary chondrocytes were isolated from the deep zone cartilage of five immature bovine knee joints (Green Village, NJ) by segregating the bottom third of articular cartilage and removing any remaining calcified cartilage [36]. Briefly, the isolated cartilage pieces were pooled and digested for 16 h with collagenase type II (3.5 activity units/mg, Worthington, Lakewood, NJ) in Dulbecco's modified Eagle's medium (DMEM) supplemented with 10% fetal bovine serum (FBS, Atlanta Biologicals, Atlanta, GA), 2% antibiotics (10,000 U/ml penicillin, 10 mg/ml streptomycin), and 0.2% antifungal (amphotericin B). The cell suspension was then filtered before plating (30 μm, Spectrum, Rancho Dominguez, CA). Isolated chondrocytes were maintained in high-density culture (4×10^5 cells/cm^2) in fully-supplemented media for 48 h before seeding [20]. All media supplements were purchased from Cellgro-Mediatech unless otherwise specified.

2.2. Agarose and agarose-hydroxyapatite scaffold fabrication

Sterile 4% agarose solution (Type VII, Sigma) was made in phosphate buffered saline (PBS) and combined 1:1 (by volume) with cell suspension (20×10^6 cells/mL). The cell-agarose mixture was cast between two glass platens and allowed to gel at room temperature for 15 min, resulting in a final seeding density of 10×10^6 cells/ml in 2% agarose. To fabricate HA-containing scaffolds, ceramic particles were first mixed with the cell suspension, then combined 1:1 with a 4% agarose solution to form 2% agarose scaffolds containing 1.5 w/v% HA. Individual disks (5 mm diameter × 2.4 mm height) were cored with a sterile biopsy punch (Sklar Instruments, West Chester, PA). Both acellular and cellular scaffolds were cultured under humidified conditions at 37 °C and 5% CO_2, maintained in ITS media consisting of DMEM supplemented with 1% ITS + Premix (BD Biosciences, San Jose, CA), 1% antibiotics, 0.1% antifungal, and 40 μg/ml proline (Sigma). The media was changed every other day and supplemented each time with fresh 50 μg/ml ascorbic acid (Sigma).

In order to induce hypertrophy, DZC were stimulated with triiodothyronine (T3, Sigma, St Louis, MO) during the first three days of culture [29]. The optimal dose was determined by assessing chondrocyte ALP activity after stimulation with 0, 10, 25,200, 1000, or 2000 nM of T3. By day 7, a significantly higher alkaline phosphatase (ALP) activity was detected for DZC cultures with 10 nM of T3 as compared to HA-free control, with the highest ALP activity observed in the 25 nM T3 group. However, no significant difference in ALP activity was measured beyond 25 nM of T3. Based on these observations, chondrocyte hypertrophy was induced by stimulation with 25 nM of T3 in this study.

The responses of DZC and DZC stimulated by T3 (DZC + T3) were compared in HA-free and HA-containing agarose scaffolds over a two-week culturing period. The effect of HA size on DZC and DZC + T3 was evaluated by comparing cell response in agarose scaffolds with micron-sized (18–28 μm, Sigma) and nano-sized (140–240 nm, Nanocerox, Ann Arbor, MI) HA particles. Next, utilizing the optimal chondrocyte population (DZC vs. DZC + T3) and HA size (micron vs. nano), the effect of ceramic dose was investigated by comparing scaffolds with 0%, 1.5%, 3.0%, or 6.0 w/v% HA. In this study, a scaffold HA content range of 0–6% by wet weight is equivalent to a range of 0–70% by dry weight. These values are

selected in order to be able to test HA doses which are lower, comparable or higher than those reported for the native interface.

2.3. Scaffold characterization

The as-fabricated scaffolds were characterized in terms of ceramic distribution, content, and chemistry. Gross morphology of the scaffolds was assessed with a stereoscope in both cross-sectional and top views. Distribution of HA particles ($n = 2$) was visualized under environmental scanning electron microscopy (ESEM, 15 kV, JEOL 5600LV, Tokyo, Japan). Scaffold water content (wet weight-dry weight/ wet weight, $n = 3$) was determined following desiccation for 24 h (CentriVap Concentrator, Labconco Co., Kansas City, MO), and ceramic content (ash weight/dry weight, $n = 3$) was measured by thermogravimetric analysis (TA Q-50, TA Instruments, New Castle, DE). The sample was heated to 100 °C, followed by a 20 °C/min ramp to 700 °C, and the residual weight was then determined. Elemental composition ($n = 2$) of the scaffolds was ascertained by energy dispersive X-ray analysis (EDAX, 15 kV, FEI Quanta 600, FEI Co., Hillsboro, OR).

The size, chemistry, as well as structure of micro-HA and nano-HA particles used in the fabrication of the composite scaffolds were also compared. The diameter ($n = 18$) of the micron-sized particles was measured directly using ImageJ. A zetasizer was used to determine the size of nano-HA (Zetasizer Nano-ZS Test Measurement System, Malvern, Worcestershire, UK). Briefly, a particle solution of 10% dextran solution and 1% HA was sonicated prior to the measurement to prevent particle aggregation. Dynamic light scattering was then used to directly measure the diffusion of particles and convert to size via the Stokes-Einstein relationship. Ceramic chemistry was examined using Fourier transform infrared spectroscopy (FTIR, FTS 3000MX Excalibur Series, Digilab, Randolph, MA), whereby the samples were air-dried in a chemical hood, and FTIR spectra were collected in absorbance mode (400 scans, resolution at 4 cm^{-1}). Finally, crystallographic structure of HA was confirmed with X-ray diffraction (XRD, X-ray Diffractometer, Inel, Artenay, France). The samples were evaluated over a range of 0–120 °, with a step size of 0.029 °.

2.4. Cell proliferation and matrix deposition

Cell proliferation ($n = 5$) was determined using the PicoGreen® total DNA assay (Molecular Probes, Eugene, OR). Briefly, the samples were lysed with 500 μl of 0.1% Triton-X solution (Sigma), and an aliquot of the sample (25 μl) was added to 175 μl of PicoGreen® working solution. Fluorescence was measured with a microplate reader (Tecan, Research Triangle Park, NC), at the excitation and emission wavelengths of 485 and 535 nm, respectively. Total cell number was obtained by converting the amount of DNA per sample to cell number using the conversion factor of 7.7 pg DNA/ cell [37].

Collagen deposition ($n = 5$) was quantified with a modified hydroxyproline assay [38]. Briefly, the samples were first desiccated for 24 h and then digested for 16 h at 60 °C with papain (600 μg protein/ml) in 0.1 M sodium acetate (Sigma), 10 mM cysteine HCl (Sigma), and 50 mM ethylenediaminetetraacetate (Sigma). A 40 μl aliquot of the digest was hydrolyzed with 10 μl of 10 M sodium hydroxide and autoclaved for 25 min. The hydrolyzate was then oxidized by a buffered chloramine-T reagent for 25 min before the addition of Ehrlich's reagent. Sample absorbance was measured at 550 nm (Tecan), and the collagen content was obtained by interpolation along a standard curve of bovine collagen I (Sigma). Additionally, collagen distribution ($n = 2$) was visualized by Picrosirius red staining. Briefly, the samples were first fixed in neutral buffered formalin and 1% cetylpyridinium chloride (Sigma) for 24 h, followed by dehydration with an ethanol series. Prior to staining and imaging, the dehydrated samples were embedded in paraffin (Type 9,

Richard-Allan Scientific, Kalamazoo, MI), sectioned from the center of the scaffold (7 m m sections), and mounted on microscope slides.

Deposition of collagens I, II, and X ($n = 2$) were evaluated using immunohisto-chemistry. Monoclonal antibodies for collagen I (1:20 dilution) and collagen II (1:100 units dilution) were purchased from Abcam (Cambridge, MA), while collagen X antibody (1:1 dilution) was obtained from the Developmental Studies Hybridoma Bank (University of Iowa). After fixation, samples were treated with 1% hyaluronidase for 30 min at 37 °C to remove proteoglycan and incubated with primary antibody overnight. A FITC-conjugated secondary antibody (1:200 dilution, LSAB2 Abcam) was used and sections were imaged via confocal microscopy at excitation and emission wavelengths of 488 nm and 568 nm, respectively.

Sample glycosaminogylcan content (GAG, $n = 5$) was determined with a modified 1,9-dimethylmethylene blue (DMMB) binding assay [39–41], with chondrotin-6-sulfate (Sigma) as the standard. The absorbance difference between 540 nm and 595 nm was used to improve the sensitivity in signal detection. Distribution of GAG ($n = 2$) was visualized by Alcian blue staining of paraffin-embedded sections [37].

2.5. Scaffold mechanical properties

Scaffold mechanical properties ($n = 3$) were determined on a shear-strain controlled rheometer (TA instruments, New Castle, DE) following published protocols [42]. Briefly, each sample was placed between two flat porous platens and immersed in DMEM to prevent dehydration. First, the equilibrium compressive Young's modulus (E_{eq}) was calculated at 15% compressive strain, which is within the physiological range for articular cartilage [43]. Secondly, a dynamic shear test was performed (0.01 Hz–10 Hz) with a logarithmic frequency sweep at a shear strain amplitude of 0.01 radian. Both the magnitude of the complex shear modulus ($|G^*|$) and phase shift angle (δ) between the applied strain and the resulting torque were determined at 1 Hz.

2.6. Mineralization and chondrocyte hypertrophy

Alkaline phosphatase (ALP) activity ($n = 5$) was quantified using an enzymatic assay based on the hydrolysis of *p*-nitrophenyl phosphate (pNP-PO_4) to *p*-nitrophenol (pNP) [44]. Briefly, the samples were lysed in 0.1% Triton-X solution, then added to pNP-PO4 solution (Sigma) and allowed to react for 30 min at 37 °C. The reaction was terminated with 0.1 N NaOH (Sigma), and sample absorbance was measured at 415 nm. In addition, mineral distribution ($n = 2$) was evaluated with Alizarin Red staining and by von Kossa staining with 5% silver nitrate, followed by 30 min of UV exposure [45]. Additionally, media calcium concentrations ($n = 5$) were quantified using the Arsenazo III dye (Pointe Scientific, Lincoln Park, MI), with absorbance measured at 620 nm using a microplate reader [46].

The expression of collagen X, matrix metalloproteinase-13 (MMP13), Indian Hedgehog *(Ihh)*, and parathyroid hormone-related protein (PTHrP) were measured at day 14 using reverse transcription followed by polymerase chain reaction (RT-PCR, $n = 3$), with custom-designed primers. The oligonucleiotide primer sequences were: GAPDH: GCTGGTGCTGAGTATGTGGT (sense), CAGAAGGTGCAGAGATGATGA (antisense); Collagen X: TGGATCCAAAGGCGATGTG (sense), GCCCAGTAGGTCCATTAAGGC (antisense); MMP13: ACATCCCAAAACGCCAGACAA (sense), GATGCAGCCGCCAGAA-GAAT (antisense); Ihh: ATCTCGGTGATGAACCAGTG (sense), CCTTCGTAATGCAGCGACT (antisense); PTHrP: ACCTCGGAGGTGTCCCCTAA (sense), GCCCTCATCATCAGACCCAA (antisense). Total RNA was isolated via TRIzol (Invitrogen) extraction, and then reverse-transcribed into cDNA using the SuperScript III First-Strand Synthesis System (Invitrogen). The cDNA

product was amplified with recombinant Platinum Taq DNA polymerase (Invitrogen). Expression band intensities of relevant genes were analyzed semi-quantitatively and normalized to the housekeeping gene glyceraldehydes 3-phosphate dehydrogenase (GAPDH). Cell size ($n = 12$) was determined by computing cell surface area from the long-axis and short-axis of individual cells (32x) at day 14.

2.7. Statistical analysis

Results are presented in the form of mean ± standard deviation, with n equal to the number of samples analyzed. Multi-way analysis of variance (ANOVA) was performed to determine the effects of T3 stimulation, HA presence and size, as well as dose and culturing time. The Tukey–Kramer *post-hoc* test was used for all pair-wise comparisons, and significance was attained at $p < 0.05$. All statistical analyses were performed using the JMP software (SAS Institute, Cary, NC). In addition, to evaluate structure-function relationships, correlations between mechanical properties (E_{eq}, $|G^*|$, δ) and scaffold collagen as well as GAG content were determined either individually (GAG or collagen) or in combination (GAG + collagen) using linear regression models [20]. Specifically, mechanical properties and matrix content from the HA-free, micro-HA, and nano-HA groups at day 14 were correlated (R^2, slope, *p*-value).

3. Results

3.1. Scaffold characterization

Acellular HA-free agarose scaffolds were compared to those with either micro-HA or nano-HA in terms of particle distribution, scaffold chemistry, and ceramic content. The HA-free and HA-containing scaffolds were visualized with environmental electron microscopy (ESEM). While the agarose scaffold was homogeneous and uniform in appearance, ceramic particles were uniformly distributed throughout the micro-HA and nano-HA scaffolds (Fig. 1A). Energy-dispersive X-ray analysis detected the presence of calcium (Ca) and phosphorus (P) peaks only in the HA-containing scaffolds (Fig. 1A).

Micro-HA and nano-HA powders were characterized in terms of ceramic chemistry and structure. Analysis by FTIR confirmed the presence of carbonate (1400–1500 cm^{-1}) peaks in both micro-HA and nano-HA, as well as peaks corresponding to three phosphate vibration modes (962 cm^{-1}, 1040–1092 cm^{-1}, 561–601 cm^{-1}, Fig. 1B). Furthermore, the 002, 211, 112, 300, 202, 301, 102, 210, and 212 crystal planes were identified in the XRD diffraction patterns of both micro-HA and nano-HA [47]. These findings confirm the similarity between the micro and nano particles in terms of chemistry and crystal structure.

As expected, scaffolds containing HA measured higher wet weight and dry weight, and therefore, lower water content as compared to HA-free controls ($p < 0.05$, Fig. 1C). While there was no difference in wet weight between the 1.5% HA and 3% HA scaffolds, a significantly higher wet weight was found with the addition of 6% HA. A dose-dependent increase in dry weight also corresponded with a dose-dependent decrease in water content ($p < 0.05$). In terms of ceramic content, no significant difference was found between the micro-HA and nano-HA scaffolds, and the 3% and 6% HA groups measured 43.8 ± 1.2% (mg HA/mg DW) and 66.3 ± 0.8% (mg HA/mg DW), respectively. The HA-free scaffolds measured a compressive modulus of 2.9 ± 0.2 kPa and magnitude of the dynamic shear modulus of 4.8 ± 0.6 kPa (Fig. 1C). While the addition of 1.5% HA and 3% HA did not significantly alter mechanical properties, the presence of 6% micro-HA resulted in a significant increase in both compressive modulus (4.3 ± 0.2 kPa) and magnitude of the dynamic shear modulus (8.7 ± 1.1 kPa). No significant difference in phase shift angle was found among any of the

groups tested. In addition, no significant difference in scaffold dimensions and mechanical properties were found between the acellular and cellular scaffolds (*data not shown*).

3.2. Effect of HA presence and size on deep zone chondrocytes

To assess the effect of ceramic presence and particle size on cell response, DZC were seeded in HA-free and HA-containing agarose scaffolds. Histological staining revealed that both cell distribution and matrix deposition were uniform throughout the depth of the scaffolds for all groups examined. Moreover, cell number remained relatively constant over time for the HA-free and nano-HA groups (Fig. 2). In contrast, a significant increase in cell number was measured for the micro-HA group during the first week of culture. By day 14, a higher cell number was found in the micro-HA group as compared to the HA-free group ($p < 0.05$), with no difference detected between the nano-HA and micro-HA groups. While no significant difference in matrix content was evident between the scaffold groups examined, a significant increase in both GAG and collagen deposition was found from day 1 to day 7 for all scaffold groups, with no further increase detected thereafter.

As expected, mineralization potential of DZC decreased over time for all groups ($p < 0.05$), with no significant difference seen between HA-free and HA-containing scaffolds. While the expression of markers relevant for chondrocyte maturation (collagen X, MMP13, *Ihh*, PTHrP), were detected in all DZC-seeded scaffolds at day 14, no significant difference was found between groups.

3.3. Effect of HA presence and size on hypertrophic chondrocytes

For the hypertrophic chondrocytes (DZC + T3), a significant increase in cell number was measured between day 7 and day 14 for the HA-free and nano-HA groups (Fig. 3). No change in cell number was found over time for the micro-HA group. At both day 7 and day 14, a significantly higher cell number was measured in the HA-free and nano-HA scaffolds as compared to micro-HA scaffolds. Proteoglycan deposition increased over the first week of culture for all groups, with no change thereafter ($p < 0.05$, Fig. 3). By day 14, significantly higher GAG content was measured in the micro-HA scaffold as compared to either nano-HA or HA-free scaffolds. While no change in collagen content was measured during the first week of culture, significant increases were observed for all groups between day 7 and day 14. The highest collagen content was found in the micro-HA group as compared to either the HA-free or nano-HA groups ($p < 0.05$). Histological staining at day 14 confirms the deposition of GAG and collagen for all groups, with strongly positive staining evident in the micro-HA scaffold. While no positive staining for collagen I was evident for any of the groups tested, collagen II staining was observed in HA-free, micro-HA, and nano-HA scaffolds after two weeks of culture.

No significant change in ALP activity was detected for hypertrophic chondrocytes in HA-free scaffolds during two weeks of culture(Fig. 4). In contrast, a decrease in ALP activity was first measured from day 1 to day 7 when these cells were cultured in HA-containing scaffolds ($p < 0.05$), followed by a significant increase in ALP activity during the second week of culture. By day 14, significantly higher ALP activity was measured in HA-containing scaffolds as compared to the HA-free group, with no difference detected between the micro-HA and nano-HA groups.

Von Kossa staining at day 14 confirms the uniform distribution of HA inside the hydrogel scaffold, as well as evidence of mineralization throughout the hydrogel (Fig. 4). A significant decrease in media calcium concentration was measured at day 14 for both acellular and cell-laden micro-HA groups as compared to plain media control. In contrast, no such change in calcium concentration was seen for the nano-HA group. Furthermore, no

significant difference in media calcium was measured between corresponding acellular and cell-laden scaffolds for both the HA-free and HA-containing groups.

Chondrocyte hypertrophy was also assessed by measuring cell size, the expression of hypertrophic markers, and deposition of collagen X. In terms of cell size, while there was no change in chondrocyte aspect ratio, the hypertrophic DZC cultured in HA-containing scaffolds measured a larger surface area by day 14 ($p < 0.05$), with no significant difference detected between the micro-HA and nano-HA groups. Collagen X expression was upregulated at day 14 for hypertrophic chondrocytes cultured in HA-containing scaffolds as compared to HA-free scaffolds. Immunohistochemistry confirmed the deposition of collagen X in HA-containing groups, with no difference found between micro-HA and nano-HA groups. While there was no difference in MMP13 and PTHrP expression between groups, *Ihh* was upregulated in the HA-containing scaffolds as compared to the HA-free scaffold ($p < 0.05$). Again, no difference in *Ihh* expression was measured between micro-HA and nano-HA groups.

3.4. Effect of HA presence and size on scaffold mechanical properties

For the hypertrophic chondrocyte-seeded groups, mechanical properties of the HA-containing scaffolds were compared to those of HA-free scaffolds at day 14. As expected, all cell-seeded scaffolds measured significantly higher compressive modulus, magnitude of the dynamic shear modulus, and phase shift angle over their corresponding acellular controls (Fig. 5). After two weeks of culture, the micro-HA group measured higher compressive and shear moduli as compared to the HA-free control ($p < 0.05$), with no statistical difference detected between the nano-HA and HA-free scaffolds. No difference in phase shift angle between the micro-HA scaffold and HA-free control was measured, although a significantly lower angle was found for the nano-HA group as compared to all other groups.

In order to determine the structure-function relationship of the hydrogel-ceramic composites, linear correlation analysis was performed for hypertrophic chondrocytes seeded in HA-free, micro-HA and nano-HA scaffolds (Fig. 5). Not surprisingly, a positive correlation between GAG and compressive modulus was observed for all scaffolds. Interestingly, higher correlation coefficients were found between GAG and compressive modulus for the micro-HA ($R^2 = 0.93$) and nano-HA groups ($R^2 = 0.83$) as compared to the HA-free group ($R^2 = 0.74$). There was also a positive correlation between GAG and magnitude of the dynamic shear modulus for all groups, which again was higher for the micro-HA ($R^2 = 0.93$) and nano-HA scaffolds ($R^2 = 0.91$) as compared to the HA-free scaffolds ($R^2 = 0.75$). With respect to the phase shift angle, a correlation with GAG was detected for the HA-free group ($R^2 = 0.67$) and micro-HA group ($R^2 = 0.86$), with no positive correlation evident in the nano-HA group.

Collagen content was also correlated to scaffold mechanical properties. Positive correlation was found between collagen and compressive modulus for HA-free ($R^2 = 0.74$) and micro-HA groups ($R^2 = 0.71$), with the highest correlation seen in the nano-HA group ($R^2 = 0.96$). Collagen content also correlated with magnitude of the dynamic shear modulus for the HA-free ($R^2 = 0.77$), micro-HA ($R^2 = 0.90$), and nano-HA ($R^2 = 0.83$) groups. Similar to GAG, collagen correlated with phase shift angle only for the HA-free ($R^2 = 0.68$) and micro-HA ($R^2 = 0.78$) groups.

Correlations were also performed with both GAG and collagen to determine their synergistic effects. No significant correlation between combined matrix content and any of the mechanical properties investigated was seen in the HA-free group. In contrast, for the micro-HA scaffolds, significant correlations were measured with combined matrix content and compressive modulus ($R^2 = 0.93$), magnitude of the dynamic shear modulus ($R^2 = 0.96$),

and phase shift angle (R^2 = 0.89). For the nano-HA group, combined matrix content also correlated with compressive modulus (R^2 = 0.97)and magnitude of the dynamic shear modulus (R^2 = 0.91).

3.5. Effect of HA dose on hypertrophic chondrocytes

Given the significantly higher ALP activity, matrix content, and mechanical properties measured with hypertrophic chondrocytes (DZC + T3) cultured in agarose scaffolds with micro-HA, scaffold design is further optimized by testing the response of DZC + T3 as a function of HA dose in (0%, 1.5%, 3%, and 6w/v% micro-HA). Significant increases in cell number were measured over time at all doses of HA, with no apparent difference found as a function of HA content (Fig. 6A). While the deposition of GAG increased over the 14-day culturing period for all groups tested ($p < 0.05$), the 1.5% and 3% HA groups measured significantly higher GAG content at day 14 as compared to the 0% HA and 6% HA groups. Similarly, collagen deposition increased between day 1 and day 14 in all scaffolds ($p < 0.05$), and significantly higher collagen content was measured in 1.5% and 3% HA scaffolds as compared to the 0% HA scaffold after two weeks of culture. No difference in collagen content was found between the 6% HA and the other groups examined. Histological staining confirmed positive and uniform deposition of GAG and collagen in all scaffolds by day 14 (Fig. 6A).

The ALP activity of hypertrophic chondrocytes cultured in HA-containing scaffolds increased significantly over time (Fig. 7). After two weeks of culture, chondrocytes in the 1.5%, 3%, and 6% HA scaffolds measured significantly higher ALP activity as compared to the 0% HA group, with the highest ALP activity found in the 3% HA group. As expected, staining intensity for both calcium (Alizarin Red) and phosphate (Von Kossa) increased with increasing HA dose. Interestingly, there was evidence of mineral deposition between pre-incorporated HA particles (Fig. 7). In terms of hyper-trophic markers, collagen X was significantly upregulated in the 3% HA scaffold as compared to the 0% HA group, with an additional four-fold increase seen in the 6% HA group by day 14. Upregulation of MMP13 was detectable only in the 6% HA scaffold ($p < 0.05$). In addition, by day 14, *Ihh* and PTHrP expression were significantly downregulated for the 3% HA and 6% HA groups as compared to the 0% HA and 1.5% HA groups.

3.6. Effect of HA dose on scaffold mechanical properties

The mechanical properties of acellular 1.5% and 3% HA scaffolds were not significantly different from those of the acellular 0% HA scaffolds by day 14, although both higher compressive and shear moduli were measured for the acellular 6% HA group ($p < 0.05$, Fig. 6B). When the scaffolds were seeded with hypertrophic chondrocytes, the 3% HA and 6% HA groups measured a higher compressive modulus than the 0% HA group ($p < 0.05$), with no significant difference seen between the 3% HA and 6% HA groups. No difference in compressive modulus was found for the 1.5% HA group as compared to the 0% HA group. In terms of the magnitude of the dynamic shear modulus, a dose-dependent increase was observed in the 1.5% HA and 3% HA groups ($p < 0.05$). The magnitude of the dynamic shear modulus of the 6% HA scaffolds was higher than that of the 0% HA or 1.5% HA scaffolds ($p < 0.05$), although it was not significantly different as compared to the 3% HA scaffold. No difference in phase shift angle was detected between the 0% HA, 1.5% HA, and 6% HA groups, although a significantly higher angle was measured for the 3% HA group at day 14 with respect to the 0% HA group.

4. Discussion

The goal of this study is to design and optimize a hydrogel-hydroxyapatite (HA) scaffold for calcified cartilage formation. To this end, the response of deep zone chondrocytes and hypertrophic chondrocytes were compared in agarose scaffolds with and without HA, and the ceramic phase was also optimized in terms of HA particle size and dose in order to promote hypertrophy and calcified matrix deposition. While ceramic presence had minimal effect on biosynthesis by deep zone chondrocytes, it significantly modulated both matrix deposition and mineralization by hyper-trophic chondrocytes. Moreover, while hypertrophy was upregulated in HA-containing hydrogels independent of ceramic size, enhanced matrix deposition was observed only in scaffolds with micron-sized HA. When the response of hypertrophic chondrocytes was further assessed as a function of micro-HA content, a dose-dependent effect on biosynthesis and the expression of hypertrophic markers was found. It was observed that chondrocyte matrix deposition, alkaline phosphatase (ALP) activity, as well as scaffold compressive and shear moduli were the highest in scaffolds containing 3% micron-sized HA particles, resulting in significant structure-function correlations between matrix content and mechanical properties of the hydrogel-ceramic scaffold.

The results of this study suggest that hypertrophic chondrocytes are more optimal for calcified cartilage regeneration in the agarose-HA scaffold. While no change in deep zone chondrocyte biosynthesis and hypertrophy were detected here in the presence of HA, hypertrophic chondrocytes exhibited enhanced mineralization potential with the addition of HA. To ascertain whether the observed effects of micro-HA are in response to ceramic presence or are merely the result of the inclusion of a particulate phase within the hydrogel matrix, the hypertrophic chondrocytes were also cultured in agarose scaffolds with inert, micron-sized glass beads. It was found that bead presence had no effect on chondrocyte biosynthesis or mineralization potential, demonstrating that the effects observed were due to HA (*data not shown*). Published studies have shown that cartilage mineralization is proceeded by accumulation of critical ions such as calcium and phosphate [48,49], it is possible that the composite hydrogelceramic scaffold can serve as a reservoir of these ions which regulate chondrocyte mineralization. This is confirmed by the precipitation of calcium from the media seen in both acellular and cellular HA-containing groups. In addition to hypertrophy and ALP activity, hypertrophic chondrocytes measured higher GAG and collagen deposition in agarose scaffolds containing micro-HA. As mineral deposits in calcified cartilage are often associated with collagen fibers [15], the elevated collagen deposition may facilitate cell-mediated mineralization. Characterization studies of growth plate cartilage has reported a localized increase in proteoglycan deposition by hypertrophic chondrocytes surrounding mineral clusters [50], whereby the proteoglycans have been postulated to serve as nucleation sites for further mineralization [51]. These results collectively suggest that cell-mediated mineralization, coupled with GAG and collagen synthesis, occurred in agarose scaffolds containing micro-HA. Not only was the total matrix content higher in scaffolds with micro-HA, both GAG and collagen synthesis per cell were significantly greater than those of the HA-free scaffolds.

It is interesting to note that while chondrocyte hypertrophy is not particle size-dependent, enhanced matrix deposition is found only when the hypertrophic chondrocytes are cultured in a hydrogel matrix containing micro-HA. These effects may be attributed to the fact that cell–ceramic interactions are significantly different for particles which are of similar size to individual cells versus those which are an order of magnitude smaller, as is the case for the nano-HA group. Furthermore, the mineral present in native calcified cartilage is reported to consist of large aggregates, which more closely approximate the micro-HA particles in size. Interestingly, higher matrix content in the micro-HA group also translated into greater mechanical properties, which is beneficial for functional cartilage repair since the native

calcified cartilage is critical for load transfer from cartilage to bone. More importantly, the strongly positive correlation found here between total matrix content and magnitude of the dynamic shear modulus in the micro-HA group is indicative of the deposition of a functional cartilage matrix, mimicking the interaction between proteoglycans and collagen which have been reported to strengthen cartilage in shear [52].

It is observed here that the response of hypertrophic chondrocytes to micro-HA is also dose-dependent. Chondrocyte ALP activity is found to be the highest in the 3% micro-HA scaffolds, accompanied by upregulated collagen X. Interestingly, PTHrP, which has been shown to suppress chondrocyte hypertrophy [36,53], is expressed at basal levels with 3% HA. It is likely that in the HA-containing agarose system, hypertrophy is being induced by multiple factors, including thyroid hormone stimulation, presence of HA, and their synergistic interactions. Moreover, the addition of 1.5% and 3% micro-HA to the hydrogel also enhances matrix deposition by hypertrophic chondrocytes relative to the HA-free control. For example, collagen deposition per cell is significantly higher for the 1.5% and 3% groups as compared to the control. Decreased biosynthesis with 6% HA may be explained by the lack of space for extensive matrix elaboration given the large number of HA particles pre-incorporated into the hydrogel. While no significant difference in matrix content between scaffolds with 1.5% and 3% HA were found at day 14, scaffold mechanical properties increased with ceramic content. It is likely that the proteoglycan-collagen network is more effectively reinforced by the greater number of ceramic particles in the 3% HA than in the 1.5% HA scaffolds.

In this study, HA was uniformly distributed throughout the agarose as upon cooling, the agarose solution sets into a gel in which chain segments are stabilized by hydrogen bonding [54], unlike the cross-linking of alginate which is limited by the rate of cation diffusion [20]. Consequently, agarose crosslinks uniformly and rapidly close to its gelation temperature (30 °C), which prevents sedimentation and results in uniform ceramic distribution within the scaffold. Furthermore, the lack of background staining for calcium or phosphorus in the agarose control confirms that this scaffold design allows for a controlled investigation of ceramic presence on chondrocytes biosynthesis. Moreover, while the as-fabricated alginate and agarose scaffolds measured comparable compressive and shear moduli, the cell-laden agarose scaffolds exhibited higher mechanical properties than the chondrocyteseeded alginate scaffolds after two weeks of culture. These effects were enhanced with the addition of HA to the hydrogel, with a nearly 10-fold increase in mechanical properties for micro-HA-containing agarose scaffolds as compared to alginate-micro-HA scaffolds.

It is also interesting to note that the response of deep zone chondrocytes varied in alginate and agarose composite scaffolds. Whereas chondrocyte hypertrophy and collagen deposition were upregulated in HA-containing alginate scaffolds, no such response was seen for deep zone chondrocytes in HA-containing agarose. In contrast, deep zone chondrocyte response in alginate closely resembles the response of hypertrophic chondrocytes in this study, which exhibited hypertrophy and elevated matrix synthesis in scaffolds containing HA. One possible explanation for the differences is that, unlike in agarose, the relatively high concentration of calcium in alginate hydrogels post cross-linking may regulate chondrocyte maturation. Wang et al. reported that activity of calcium-sensing receptors by extracellular calcium coincides with an increase in collagen X expression and ALP activity in CFK2 cells [55]. The addition of calcium chloride has also been shown to increase collagen X synthesis by hypertrophic chondrocytes [56]. Therefore, while the agarose system which has significant functional advantages over alginate, the addition of a bioactive ceramic which releases mineral inductive ions may further enhance the responses observed in this study, and their effects will be investigated in future studies.

Calcified cartilage formation is in general the result of chondrocyte hypertrophy and mineralization within a proteoglycan-and collagen-rich matrix. In this study, an optimal HA content and size were identified, as the hypertrophic chondrocytes produced a matrix rich in proteoglycan and collagen within the composite scaffold containing 3.0 w/v% of micron-sized HA particles. These responses are likely due to the fact that the mineral content of the 3.0% HA group most closely approximates that of native tissue [31], and micron-size aggregates are abundant at the osteochondral interface [32]. The addition of the biomimetic mineral phase within the scaffold not only modulates chondrocyte biosynthesis and hypertrophy, it also minimizes the need for extensive cell-mediated mineral deposition. Furthermore, the hydrogel-ceramic scaffold recapitulates biomimetic synergy between proteoglycan and collagen, resulting in physiologically relevant structure-function relationships which are likely beneficial for clinical implementation.

Clinically, it is envisioned that the hydrogel-ceramic scaffold may be utilized in combination with hydrogel-based cartilage tissue engineering grafts, whereby the ceramic phase promotes calcified cartilage formation and osteointegration, and the hydrogel phase of the composite facilitates integration with a hydrogel-based cartilage graft. Future studies will focus on optimizing the composite hydrogel scaffold system in terms of cell seeding density and mineral chemistry, with the long-term goal of achieving functional and integrative cartilage repair.

5. Conclusions

This study compares the response of deep zone chondrocytes and hypertrophic chondrocytes cultured in HA-free and HA-containing agarose scaffolds. The ceramic phase of scaffold was optimized by testing both HA particle size and dose. Although deep zone chondrocyte response was not affected by either ceramic presence or size, hypertrophic chondrocytes exhibited higher ALP activity in the presence of HA and deposited more proteoglycan and collagen in the hydrogel-ceramic scaffolds with micro-HA versus nano-HA particles. In terms of ceramic dose, the 3% micro-HA group is optimal for calcified cartilage formation, measuring the highest matrix content, mineralization, and mechanical properties. These results demonstrate that the optimized hydrogel-ceramic composite supported the formation of a calcified cartilage-like matrix.

Acknowledgments

The authors would like to thank Professor Van C. Mow (Columbia University, NY) for use of the rheometer system, as well as Stephen Doty, Ph.D. and Anthony Labissiere (Hospital for Special Surgery, NY) for their assistance with environmental SEM. This study was funded by the Wallace H. Coulter Foundation (HHL), NIH-NIAMS 5R01AR055280 (HHL), NIH Ruth L. Kirschstein National Research Service Award T32 AR059038 (NTK), and the National Science Foundation Graduate Research Fellowship (NTK).

References

1. Hunziker EB. Biologic repair of articular cartilage. Defect models in experimental animals and matrix requirements. Clin Orthop Relat Res. 1999:S135–S146. [PubMed: 10546642]
2. Frisbie DD, Trotter GW, Powers BE, Rodkey WG, Steadman JR, Howard RD, et al. Arthroscopic subchondral bone plate microfracture technique augments healing of large chondral defects in the radial carpal bone and medial femoral condyle of horses. Vet Surg. 1999; 28:242–255. [PubMed: 10424704]
3. Bedi A, Feeley BT, Williams RJ III. Management of articular cartilage defects of the knee. J Bone Joint Surg Am. 2010; 92:994–1009. [PubMed: 20360528]
4. Hunziker EB. Articular cartilage repair: basic science and clinical progress. A review of the current status and prospects. Osteoarthritis Cartilage. 2002; 10:432–463. [PubMed: 12056848]

5. Malmonge SM, Zavaglia CA, Belangero WD. Biomechanical and histological evaluation of hydrogel implants in articular cartilage. Braz J Med Biol Res. 2000; 33:307–312. [PubMed: 10719382]
6. Hoemann CD, Sun J, Legare A, McKee MD, Buschmann MD. Tissue engineering of cartilage using an injectable and adhesive chitosan-based cell-delivery vehicle. Osteoarthritis Cartilage. 2005; 13:318–329. [PubMed: 15780645]
7. Holland TA, Bodde EW, Cuijpers VM, Baggett LS, Tabata Y, Mikos AG, et al. Degradable hydrogel scaffolds for in vivo delivery of single and dual growth factors in cartilage repair. Osteoarthritis Cartilage. 2007; 15:187–197. [PubMed: 16965923]
8. Lind M, Larsen A, Clausen C, Osther K, Everland H. Cartilage repair with chondrocytes in fibrin hydrogel and MPEG polylactide scaffold: an in vivo study in goats. Knee Surg Sports Traumatol Arthrosc. 2008; 16:690–698. [PubMed: 18418579]
9. Schagemann JC, Erggelet C, Chung HW, Lahm A, Kurz H, Mrosek EH. Cell-laden and cell-free biopolymer hydrogel for the treatment of osteochondral defects in a sheep model. Tissue Eng Part A. 2009; 15:75–82. [PubMed: 18783325]
10. Yasuda K, Kitamura N, Gong JP, Arakaki K, Kwon HJ, Onodera S, et al. A novel double-network hydrogel induces spontaneous articular cartilage regeneration in vivo in a large osteochondral defect. Macromol Biosci. 2009; 9:307–316. [PubMed: 19031389]
11. Chao PH, Yodmuang S, Wang X, Sun L, Kaplan DL, Vunjak-Novakovic G. Silk hydrogel for cartilage tissue engineering. J Biomed Mater Res B Appl Biomater. 2010; 95:84–90. [PubMed: 20725950]
12. Roberts JJ, Nicodemus GD, Greenwald EC, Bryant SJ. Degradation improves tissue formation in (un)loaded chondrocyte-laden hydrogels. Clin Orthop Relat Res. 2011; 469:2725–2734. [PubMed: 21347817]
13. Havelka S, Horn V, Spohrova D, Valouch P. The calcified-noncalcified cartilage interface: the tidemark. Acta Biol Hung. 1984; 35:271–279. [PubMed: 6242456]
14. Norrdin RW, Kawcak CE, Capwell BA, McIlwraith CW. Calcified cartilage morphometry and its relation to subchondral bone remodeling in equine arthrosis. Bone. 1999; 24:10–14.
15. Boskey AL. Mineral-matrix interactions in bone and cartilage. Clin Orthop Relat Res. 1992:244–274. [PubMed: 1323440]
16. Redler I, Mow VC, Zimny ML, Mansell J. The ultrastructure and biomechanical significance of the tidemark of articular cartilage. Clin Orthop Relat Res. 1975; 112:357–362. [PubMed: 1192647]
17. Bullough PG, Jagannath A. The morphology of the calcification front in articular cartilage. Its significance in joint function. J Bone Joint Surg Br. 1983; 65:72–78. [PubMed: 6337169]
18. Oegema TR Jr, Carpenter RJ, Hofmeister F, Thompson RC Jr. The interaction of the zone of calcified cartilage and subchondral bone in osteoarthritis. Microsc Res Tech. 1997; 37:324–332. [PubMed: 9185154]
19. Hunziker EB, Driesang IM, Saager C. Structural barrier principle for growth factor-based articular cartilage repair. Clin Orthop Relat Res. 2001:S182–S189. [PubMed: 11603703]
20. Khanarian NT, Jiang J, Wan LQ, Mow VC, Lu HH. A hydrogel-mineral composite scaffold for osteochondral interface tissue engineering. Tissue Eng Part A. 2012; 18:533–545. [PubMed: 21919797]
21. Buschmann MD, Gluzband YA, Grodzinsky AJ, Kimura JH, Hunziker EB. Chondrocytes in agarose culture synthesize a mechanically functional extracellular matrix. J Orthop Res. 1992; 10:745–758. [PubMed: 1403287]
22. Mauck RL, Soltz MA, Wang CC, Wong DD, Chao PH, Valhmu WB, et al. Functional tissue engineering of articular cartilage through dynamic loading of chondrocyte-seeded agarose gels. J Biomech Eng. 2000; 122:252–260. [PubMed: 10923293]
23. Ng KW, Wang CC, Mauck RL, Kelly TA, Chahine NO, Costa KD, et al. A layered agarose approach to fabricate depth-dependent inhomogeneity in chondrocyte-seeded constructs. J Orthop Res. 2005; 23:13–41.
24. Jiang J, Tang A, Ateshian GA, Guo XE, Hung CT, Lu HH. Bioactive stratified polymer ceramic-hydrogel scaffold for integrative osteochondral repair. Ann Biomed Eng. 2010; 38:2183–2196. [PubMed: 20411332]

25. Ng KW, Lima EG, Bian L, O'Conor CJ, Jayabalan PS, Stoker AM, et al. Passaged adult chondrocytes can form engineered cartilage with functional mechanical properties: a canine model. Tissue Eng Part A. 2010; 16:1041–1051. [PubMed: 19845465]
26. Allan KS, Pilliar RM, Wang J, Grynpas MD, Kandel RA. Formation of biphasic constructs containing cartilage with a calcified zone interface. Tissue Eng. 2007; 13:167–177. [PubMed: 17518590]
27. Kandel RA, Hurtig M, Grynpas M. Characterization of the mineral in calcified articular cartilagenous tissue formed in vitro. Tissue Eng. 1999; 5:25–34. [PubMed: 10207187]
28. Sun Y, Kandel R. Deep zone articular chondrocytes in vitro express genes that show specific changes with mineralization. J Bone Miner Res. 1999; 14:1916–1925. [PubMed: 10571692]
29. Gannon JM, Walker G, Fischer M, Carpenter R, Thompson RC Jr, Oegema TR Jr. Localization of type X collagen in canine growth plate and adult canine articular cartilage. J Orthop Res. 1991; 9:485–494. [PubMed: 2045975]
30. Alini M, Kofsky Y, Wu W, Pidoux I, Poole AR. In serum-free culture thyroid hormones can induce full expression of chondrocyte hypertrophy leading to matrix calcification. J Bone Miner Res. 1996; 11:105–113. [PubMed: 8770703]
31. Linsenmayer TF, Long F, Nurminskaya M, Chen Q, Schmid TM. Type X collagen and other up-regulated components of the avian hypertrophic cartilage program. Prog Nucleic Acid Res Mol Biol. 1998; 60:79–109. [PubMed: 9594572]
32. Zizak I, Roschger P, Paris O, Misof BM, Berzlanovich A, Bernstorff S, et al. Characteristics of mineral particles in the human bone/cartilage interface. J Struct Biol. 2003; 141:208–217. [PubMed: 12648567]
33. Brown RA, Blunn GW, Salisbury JR, Byers PD. Two patterns of calcification in primary (physeal) and secondary (epiphyseal) growth cartilage. Clin Orthop Relat Res. 1993:318–324. [PubMed: 8358937]
34. Gupta HS, Schratter S, Tesch W, Roschger P, Berzlanovich A, Schoeberl T, et al. Two different correlations between nanoindentation modulus and mineral content in the bone-cartilage interface. J Struct Biol. 2005; 149:138–148. [PubMed: 15681230]
35. Ferguson VL, Bushby AJ, Boyde A. Nanomechanical properties and mineral concentration in articular calcified cartilage and subchondral bone. J Anat. 2003; 203:191–202. [PubMed: 12924819]
36. Jiang J, Leong NL, Mung JC, Hidaka C, Lu HH. Interaction between zonal populations of articular chondrocytes suppresses chondrocyte mineralization and this process is mediated by PTHrP. Osteoarthritis Cartilage. 2008; 16:70–82. [PubMed: 17644010]
37. Jiang J, Nicoll SB, Lu HH. Co-culture of osteoblasts and chondrocytes modulates cellular differentiation in vitro. Biochem Biophys Res Commun. 2005; 338:762–770. [PubMed: 16259947]
38. Reddy GK, Enwemeka CS. A simplified method for the analysis of hydroxyproline in biological tissues. Clin Biochem. 1996; 29:225–229. [PubMed: 8740508]
39. Enobakhare BO, Bader DL, Lee DA. Quantification of sulfated glycosaminoglycans in chondrocyte/alginate cultures, by use of 1,9-dimethylmethylene blue. Anal Biochem. 1996; 243:189–191. [PubMed: 8954546]
40. Farndale RW, Sayers CA, Barrett AJ. A direct spectrophotometric microassay for sulfated glycosaminoglycans in cartilage cultures. Connect Tissue Res. 1982; 9:247–248. [PubMed: 6215207]
41. Seibel MJ, Macaulay W, Jelsma R, Saed-Nejad F, Ratcliffe A. Antigenic properties of keratan sulfate: influence of antigen structure, monoclonal antibodies, and antibody valency. Arch Biochem Biophys. 1992; 296:410–418. [PubMed: 1378715]
42. Wan LQ, Jiang J, Miller DE, Guo XE, Mow VC, Lu HH. Matrix deposition modulates the viscoelastic shear properties of hydrogel-based cartilage grafts. Tissue Eng Part A. 2011; 17:1111–1122. [PubMed: 21142626]
43. Armstrong CG, Bahrani AS, Gardner DL. In vitro measurement of articular cartilage deformations in the intact human hip joint under load. J Bone Joint Surg Am. 1979; 61:744–755. [PubMed: 457718]

44. Lu HH, Kofron MD, El Amin SF, Attawia MA, Laurencin CT. In vitro bone formation using muscle-derived cells: a new paradigm for bone tissue engineering using polymer-bone morphogenetic protein matrices. Biochem Bio-phys Res Commun. 2003; 305:882–889.
45. Wang IE, Lu HH. Role of cell-cell interactions on the regeneration of soft tissue-to-bone interface. Conf Proc IEEE Eng Med Biol Soc. 2006; 1:783–786. [PubMed: 17946859]
46. Lu HH, Tang A, Oh SC, Spalazzi JP, Dionisio K. Compositional effects on the formation of a calcium phosphate layer and the response of osteoblast-like cells on polymer-bioactive glass composites. Biomaterials. 2005; 26:6323–6334. [PubMed: 15919111]
47. Gadaleta SJ, Paschalis EP, Betts F, Mendelsohn R, Boskey AL. Fourier transform infrared spectroscopy of the solution-mediated conversion of amorphous calcium phosphate to hydroxyapatite: new correlations between X-ray diffraction and infrared data. Calcif Tissue Int. 1996; 58:9–16. [PubMed: 8825233]
48. Wu LN, Ishikawa Y, Sauer GR, Genge BR, Mwale F, Mishima H, et al. Morphological and biochemical characterization of mineralizing primary cultures of avian growth plate chondrocytes: evidence for cellular processing of Ca2+ and Pi prior to matrix mineralization. J Cell Biochem. 1995; 57:218–237. [PubMed: 7759559]
49. Mwale F, Tchetina E, Wu CW, Poole AR. The assembly and remodeling of the extracellular matrix in the growth plate in relationship to mineral deposition and cellular hypertrophy: an in situ study of collagens II and IX and proteoglycan. J Bone Miner Res. 2002; 17:275–283. [PubMed: 11811558]
50. Shepard N, Mitchell N. Ultrastructural modifications of proteoglycans coincident with mineralization in local regions of rat growth plate. J Bone Joint Surg Am. 1985; 67:455–464. [PubMed: 3972871]
51. Gomez S, Lopez-Cepero JM, Silvestrini G, Bonucci E. Matrix vesicles and focal proteoglycan aggregates are the nucleation sites revealed by the lanthanum incubation method: a correlated study on the hypertrophic zone of the rat epiphyseal cartilage. Calcif Tissue Int. 1996; 58:273–282. [PubMed: 8661960]
52. Zhu W, Iatridis JC, Hlibczuk V, Ratcliffe A, Mow VC. Determination of collagen-proteoglycan interactions in vitro. J Biomech. 1996; 29:773–783. [PubMed: 9147974]
53. Kronenberg HM. PTHrP and skeletal development. Ann N Y Acad Sci. 2006; 1068:1–13. [PubMed: 16831900]
54. Stellwagen J, Stellwagen NC. Internal structure of the agarose-gel matrix. J Phys Chem. 1995; 99:4247–4251.
55. Wang D, Canaff L, Davidson D, Corluka A, Liu H, Hendy GN, et al. Alterations in the sensing and transport of phosphate and calcium by differentiating chondrocytes. J Biol Chem. 2001; 276:33995–34005. [PubMed: 11404353]
56. Bonen DK, Schmid TM. Elevated extracellular calcium concentrations induce type X collagen synthesis in chondrocyte cultures. J Cell Biol. 1991; 115:1171–1178. [PubMed: 1955460]

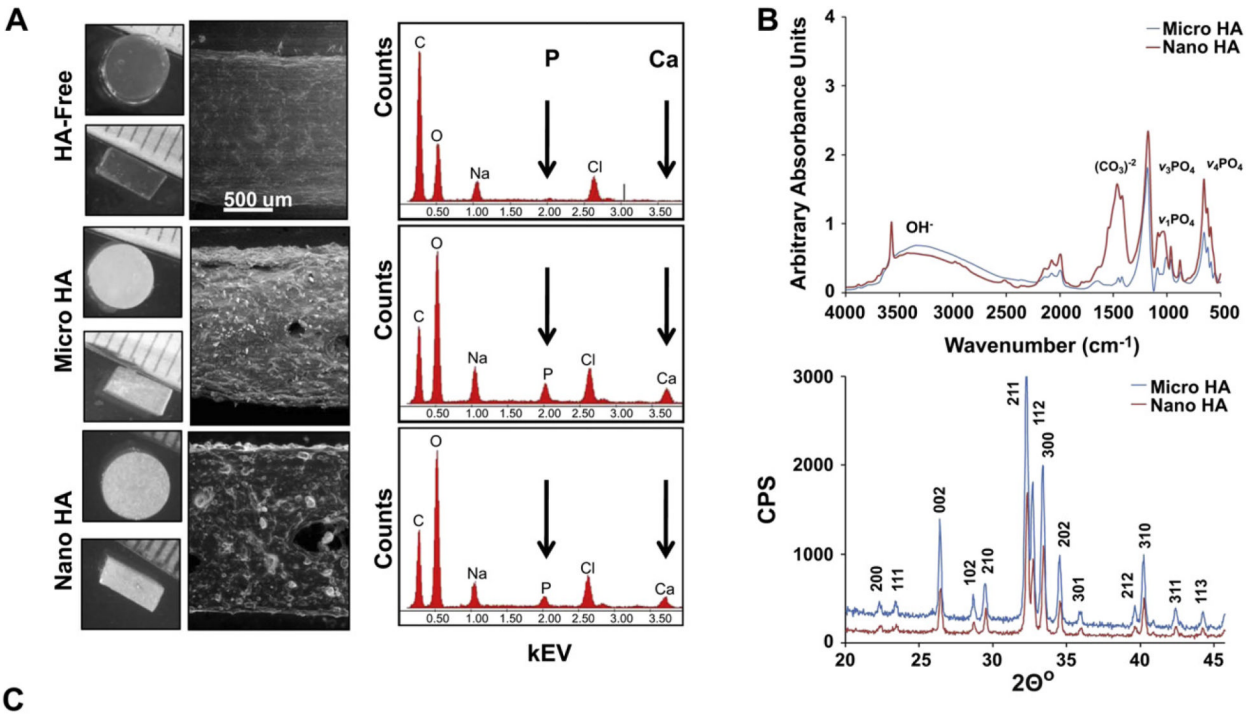

C

Day 1, Acell	WW (mg)	% Water	DW (mg)	% Ceramic	HA Size (μm)	E (kPa)	|G*| (kPa)	δ(degrees)
HA-Free	38.5 ± 2.7	98.3 ± 0.7	0.7 ± 0.3	N/A	N/A	2.9 ± 0.2	4.8 ± 0.6	0.9 ± 0.7
1.5% Nano HA	**42.7 ± 0.9***	**96.7 ± 0.4***	**1.4 ± 0.2***	27.8 ± 5.6	0.19 ± 0.05	3.5 ± 0.9	5.3 ± 0.8	2.1 ± 1.5
1.5% Micro HA	**42.6 ± 2.0***	**97.0 ± 0.3***	**1.3 ± 0.1***	26.9 ± 1.7	23.54 ± 5.62	3.1 ± 0.2	4.7 ± 0.8	1.5 ± 0.3
3% Micro HA	**45.0 ± 1.2***	**95.1 ± 0.5****	**2.2 ± 0.3****	**43.8 ± 1.2****	23.54 ± 5.62	3.6 ± 0.5	4.6 ± 0.6	2.7 ± 1.1
6% Micro HA	**46.7 ± 1.6****	**91.6 ± 1.1*****	**3.9 ± 0.4*****	**66.3 ± 0.8*****	23.54 ± 5.62	**4.3 ± 0.2***	**8.7 ± 1.1*****	1.7 ± 0.4

Fig. 1.

Scaffold characterization. (A) Light microscopy images of HA-free and HA-containing scaffolds (top-view and side-view). There is no change in scaffold dimensions ($n = 5$) with the addition of HA particles. Environmental Scanning Electron Microscopy (ESEM, 100x) reveals uniform particle distribution and Energy Dispersive X-ray Analysis (EDAX) confirms the presence of calcium (Ca) and phosphorus (P) in the HA-containing scaffolds. (B) Fourier Infrared Spectroscopy (FTIR) and X-ray Diffraction confirms that there are no difference in chemistry and crystallinity between micro-HA and nano-HA. (C) The addition of HA resulted in a dose-dependent decrease in scaffold water content (*$p < 0.05$: relative to HA-free, **$p < 0.05$: relative to HA-free and 1.5% HA groups, ***relative to HA-free, 1.5%, and 3% HA groups). Significant increases in compressive modulus (*$p < 0.05$, $n = 3$) and magnitude of the dynamic shear modulus (***$p < 0.05$, n = 3) were found for the 6% HA group.

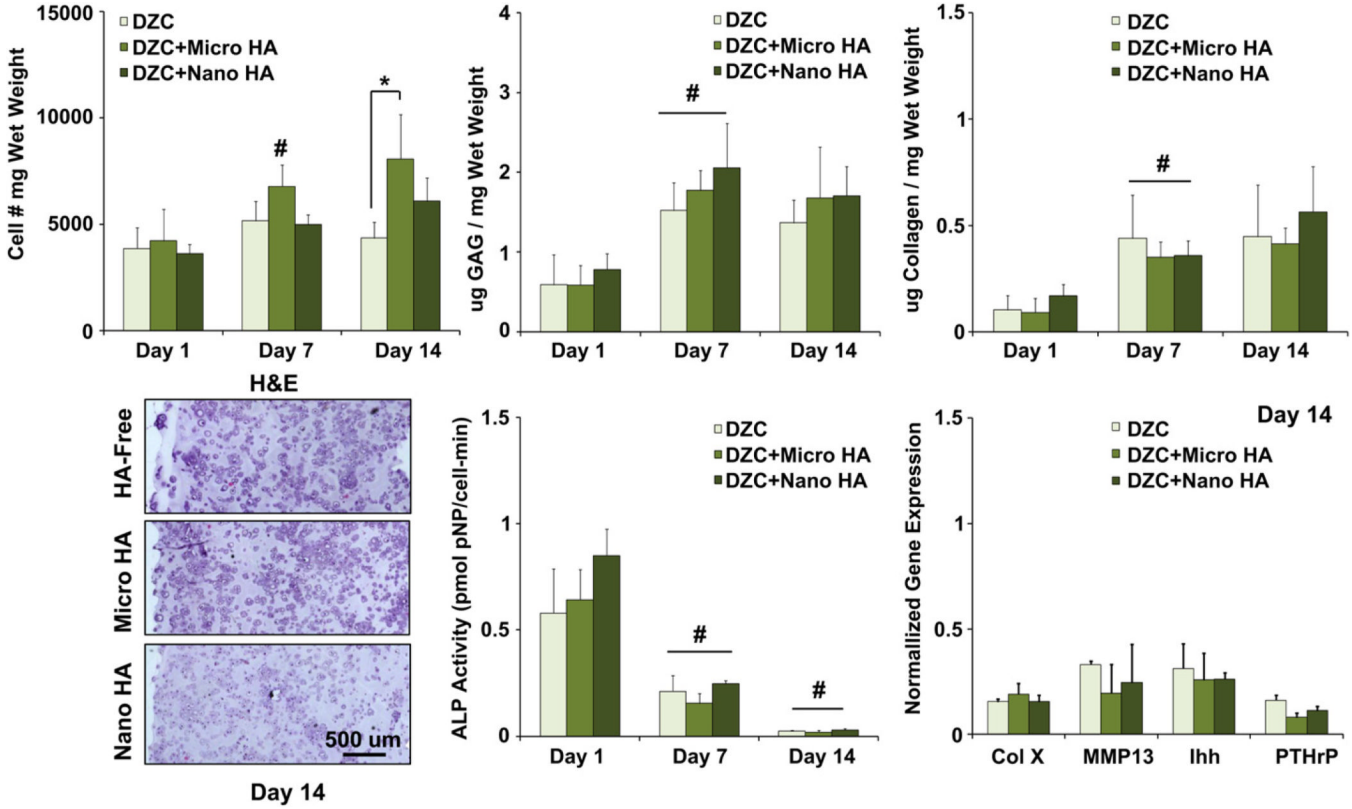

Fig. 2.

Effect of HA presence and size on deep zone chondrocytes. A higher cell number was measured at day 14 for the micro-HA group as compared to HA-free control (*$p < 0.05$, $n = 5$). Both cells and matrix are uniformly distributed throughout the scaffolds (H&E, 10x, bar = 500 μm, Day 14, $n = 2$), and GAG as well as collagen content increased for all groups over the first week of culture (#$p < 0.05$, $n = 5$). Cell ALP activity decreased over time for all groups (#$p < 0.05$, $n = 5$), with no change detected in the expression of hypertrophic markers due to either the presence or size of HA particles ($n = 3$).

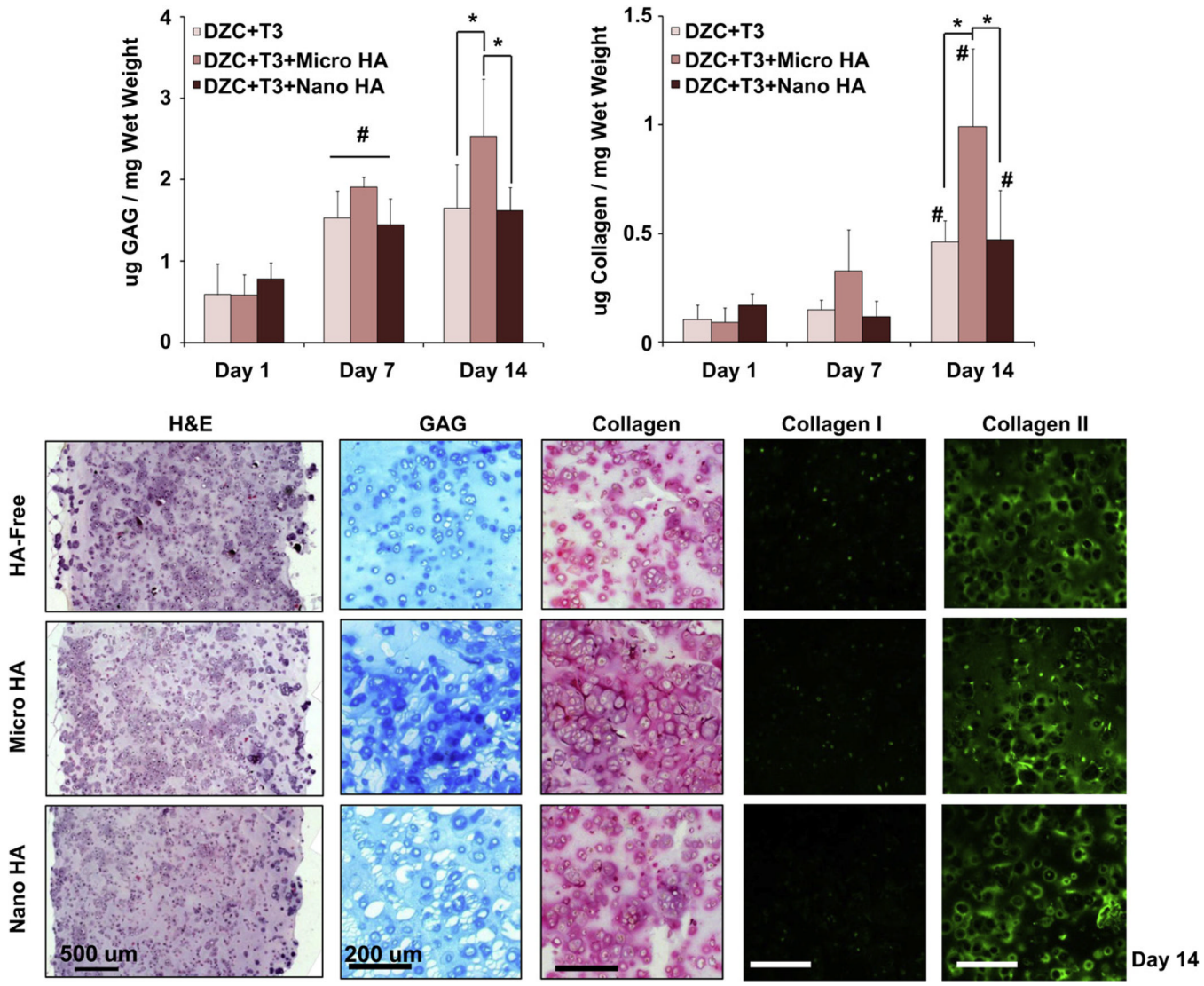

Fig. 3.

Effect of HA presence and size on hypertrophic chondrocytes: biosynthesis. Both GAG and collagen content were significantly higher at day 14 for the micro-HA group (*$p < 0.05$, $n = 5$). Corresponding histology reveals strongly positive matrix staining for the micro-HA group (Alcian Blue for GAG and Picrosirius Red for collagen, 10x, bar = 200 μm, day 14, $n = 2$). More specifically, strongly positive collagen II staining and minimal collagen I staining, was observed for all groups (immunohistochemistry, 10x, bar = 200 μm, Day 14, $n = 2$).

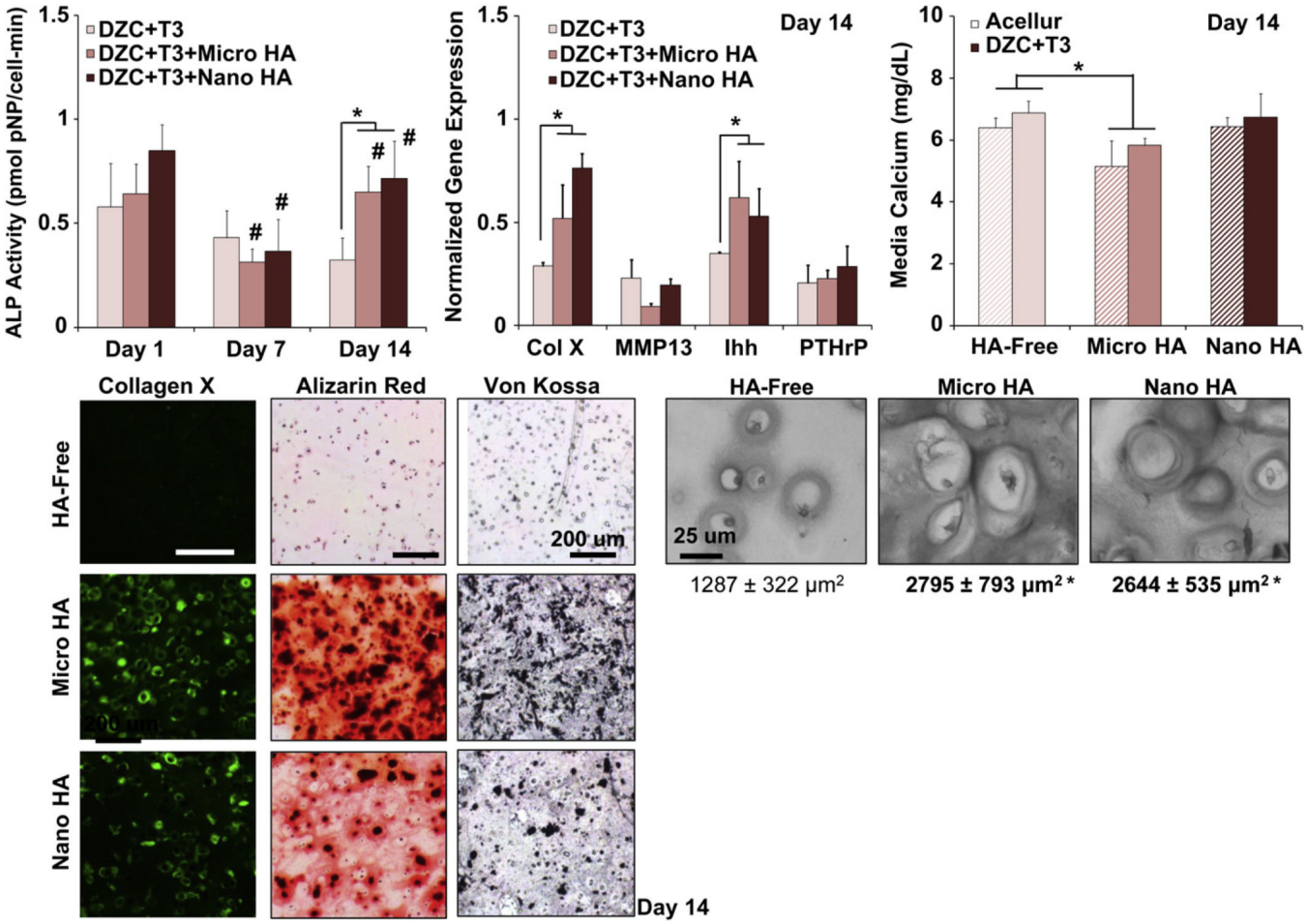

Fig. 4.

Effect of HA presence and size on hypertrophic chondrocyte: mineralization. The presence of HA significantly elevated ALP activity in hypertrophic chondrocytes by day 14 (*$p <$ 0.05, $n = 5$), with a corresponding increase in cell size in the HA-containing scaffolds (*$p <$ 0.05, bar = 25 μm, 32x, $n = 12$). Both type X collagen and *Ihh* expression are upregulated by day 14 (*$p < 0.05$, $n = 3$), with positive staining for type X collagen found at day 14 in the HA-containing scaffolds independent of particle size (10x, bar = 200 μm, $n = 2$). A significant decrease in media calcium was only found for the acellular and cell-laden micro-HA groups as compared to plain media control (*$p < 0.05$, $n = 5$), with no difference seen due to HA size. Von Kossa and Alizarin Red staining confirm the uniform distribution of HA particles in the HA-containing scaffolds, with strongly positive mineral staining seen in the micro-HA group (10x, bar = 200 μm, Day 14, $n = 2$).

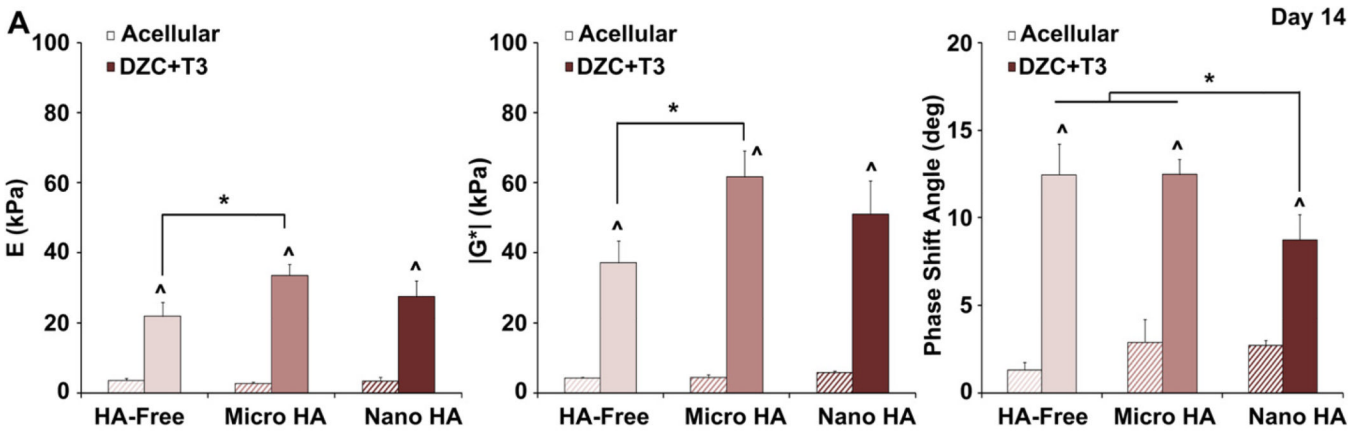

B

Linear Correlations		Compressive Modulus (E)			Shear Modulus (|G*|)			Phase Shift Angle (δ)		
		GAG	Col	GAG+Col	GAG	Col	GAG+Col	GAG	Col	GAG+Col
HA-Free	Slope	36.72	30.79	---	57.20	48.43	---	16.08	13.54	---
	R^2	0.74	0.74	0.79	0.75	0.77	0.81	0.67	0.68	0.72
	p-value	0.03*	0.03*	0.10	0.03*	0.02*	0.08	0.05*	0.04*	0.15
Micro HA	Slope	44.20	43.56	46.22, -2.57	95.98	106.38	72.70, 32.36	9.69	10.38	7.31, 3.30
	R^2	0.93	0.71	0.93	0.93	0.90	0.96	0.86	0.78	0.89
	p-value	<0.01*	0.03*	0.02*	<0.01*	<0.01*	0.01*	0.01*	0.02*	0.04*
Nano HA	Slope	43.65	58.77	-17.96, 80.39	88.86	104.18	90.48, -4.73	---	---	---
	R^2	0.83	0.96	0.97	0.91	0.83	0.91	0.04	0.02	0.10
	p-value	0.01*	<0.01*	<0.01*	<0.01*	0.01*	0.03*	0.69	0.79	0.86

Fig. 5.

Effect of HA presence and size on hypertrophic chondrocytes: scaffold mechanical properties. (A) The micro-HA containing scaffold measured a higher compressive modulus and magnitude of the dynamic shear modulus as compared to the HA-free control (*$p <$ 0.05, Day 14), and the addition of nano-HA resulted in a lower phase shift angle (*$p < 0.05$). Note that mechanical properties of all cell-laden scaffolds were significantly higher than those of the corresponding acellular controls (^$p < 0.05$, Day 14, $n = 3$). (B) For the micro-HA group, linear regression analysis revealed a strong positive correlation between scaffold mechanical properties (E, |G*|, and δ) and matrix content (GAG, Col) as well as matrix interactions (GAG + Col)(*$p < 0.05$, Day 14, $n = 6$).

A

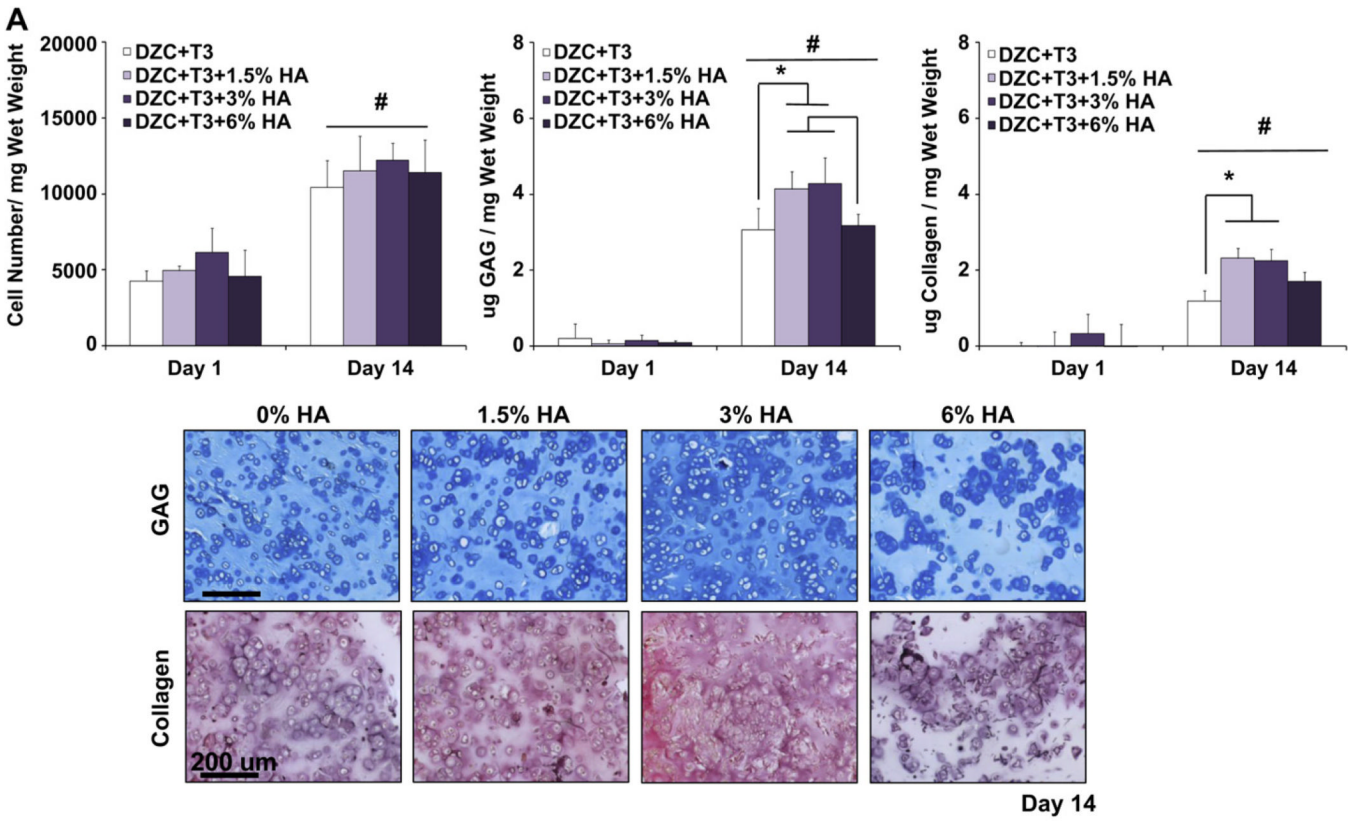

B

Day 14	Acellular				Cell-Seeded			
	0%	1.5%	3%	6%	0%	1.5%	3%	6%
E (kPa)	3.6±0.6	2.7±0.5	2.6±1.1	**5.4±0.4***	21.9±4.0	27.5±4.5	**27.1±1.5***	**26.8±2.3***
|G*| (kPa)	4.3±0.2	4.5±0.6	4.3±0.3	**8.5±0.9***	37.1±6.2	**61.7±7.4***	**75.5±8.5****	**82.9±13.0****
δ (deg)	1.3±0.4	2.9±1.3	1.0±0.5	2.7±0.7	12.4±1.8	12.5±0.9	**14.1±0.6***	13.5±1.0

Fig. 6.

Effect of HA dose on hypertrophic chondrocytes: growth, biosynthesis and scaffold mechanical properties. (A) While there is no dose-dependent effect on cell growth, the addition of 1.5% and 3% micro-HA resulted in higher GAG and collagen deposition by day 14 (*$p < 0.05$, $n = 5$), as confirmed by histology (Alcian Blue for GAG and Picrosirius Red for collagen 10x, bar = 200 μm, Day 14, $n = 2$). (B) Cell-laden scaffolds measured significantly higher compressive modulus, magnitude of the dynamic shear modulus, and phase shift angle as compared to corresponding acellular controls at day 14 ($n = 3$). A dose-dependent increase in scaffold compressive and shear moduli was found, with those of the 3% and 6% HA groups being significantly higher than that of the 0% HA group (*$p < 0.05$, $n = 3$). In addition, cell-laden scaffolds with 3% HA measured a higher phase shift angle as compared to the 0% HA group (*$p < 0.05$, $n = 3$).

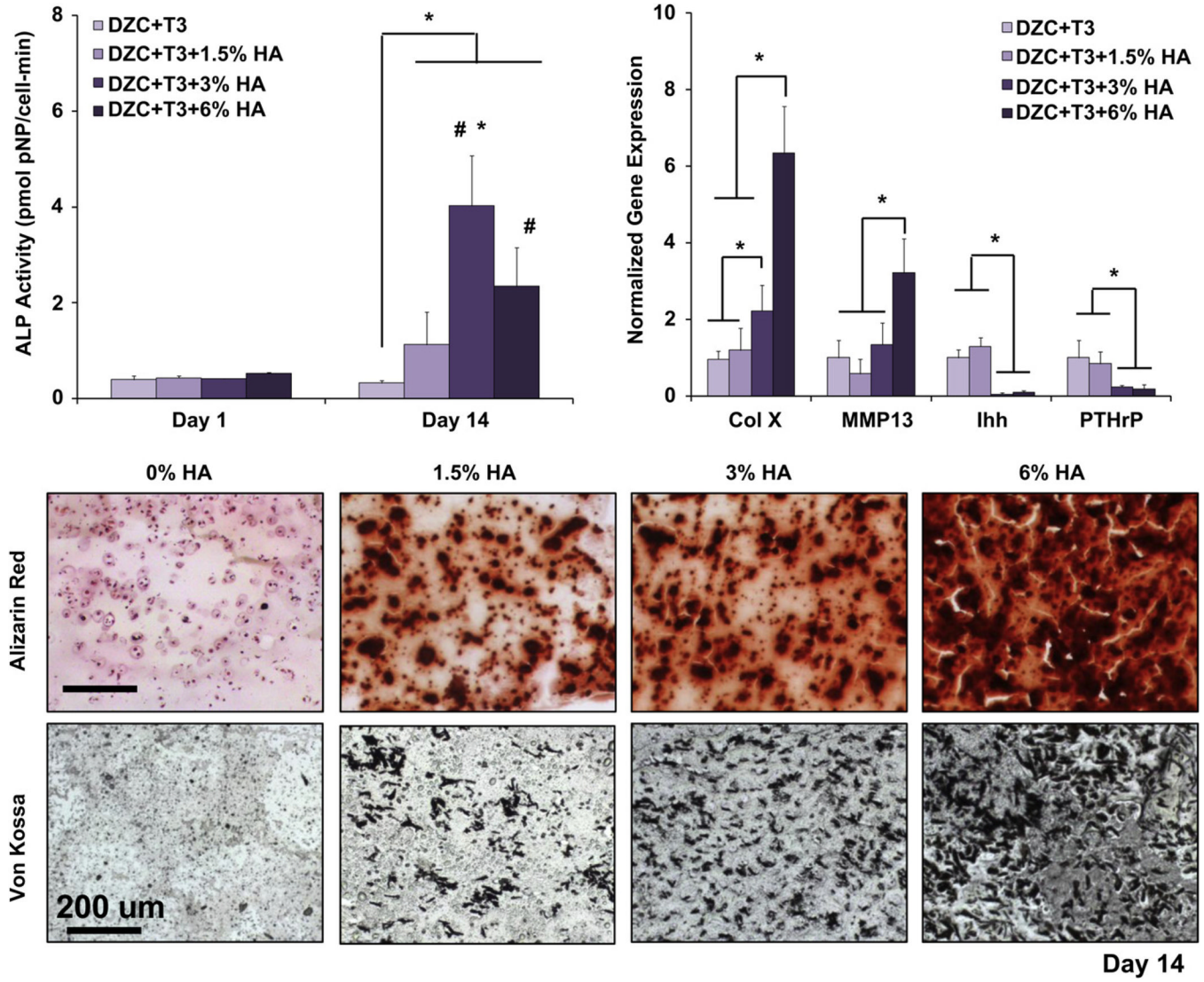

Fig. 7.

Effect of HA dose on hypertrophic chondrocytes: mineralization. A dose-dependent effect in ALP activity was found, with the highest enzyme activity detected in the 3% HA groups (*$p < 0.05$, $n = 5$). Cell ALP activity also increased over time for both the 3% and 6% HA groups (#$p < 0.05$, $n = 5$). Similarly, a dose-dependent increase in type X collagen expression was found, with the highest collagen X and MMP13 expression detected in the 6% HA group by day 14. In contrast, significant suppression of PTHrP and *Ihh* expression was found at the higher HA doses (3% and 6% HA, *$p < 0.05$, $n = 3$ normalized to 0% group). For mineralization, both von Kossa and Alizarin Red staining revealed the presence of pre-incorporated HA particles, as well as cell-mediated mineral deposition (10x, bar = 200 μm, Day 14, $n = 2$).